Clays and Clay Minerals, Vol. 56, No. 1, 112–127, 2008.

PYROXENE WEATHERING TO SMECTITE: CONVENTIONAL AND CRYO-FIELD EMISSION SCANNING ELECTRON MICROSCOPY, KOUA BOCCA ULTRAMAFIC COMPLEX, IVORY COAST

MICHAEL A. VELBEL[1,*] AND WILLIAM W. BARKER[2]

[1] Department of Geological Sciences, 206 Natural Science Building, Michigan State University, East Lansing, MI, 48824-1115, USA
[2] Department of Geology and Geophysics, University of Wisconsin-Madison, Madison, WI, 53706, USA

Abstract—Air-dried and high-pressure frozen/freeze-etched samples of clinopyroxene and smectite in a saprolitized clinopyroxenite from Koua Bocca, Ivory Coast, West Africa, were compared to characterize textures developed during natural weathering of chain silicates. Comparison with air-dried material allowed evaluation of high-pressure cryofixation as a technique for preserving textures of hydrated clay minerals. Air-dried pyroxene surfaces appear very smooth. Small, flat lamellae, oriented parallel to the *c* axis, lend a distinct splintery appearance to pyroxene surfaces in fully hydrated samples. These lamellae often display a combination of straight (110) pyroxene edges and a crinkled border, suggestive of smectite. Narrow lenticular (110) open cleavages occur in both preparations and are not a pressurization artifact. Most often these openings contain no secondary minerals. Spaces between pyroxene denticles, lined with collapsed smectite in air-dried samples, are filled with thin packets of anhedral smectite crystallites oriented face to face when hydrated. Smectite microboxwork preserves original topotactic textures developed during isovolumetric pyroxene transformation, and smaller nanoporosity appears in hydrated cryofixed examples. Occasional regions of edge-to-face 'house of cards' texture also occur. Elimination of sample preparation artifacts induced by surface tension during air drying demonstrates that pores actually present during a hydration reaction-driven weathering episode are smaller and more numerous than would be inferred from examining air-dried materials.

Key Words—Etch Pits, FEG-SEM, Isovolumetric Weathering, Pyroxene, SEM, Smectite, Weathering.

INTRODUCTION

The rate of the hydration reaction by which pyroxene weathers to smectite depends in part upon the ease with which water can diffuse to, and dissolved constituents not incorporated into smectite can diffuse away from, reacting mineral surfaces. Even if diffusion through the weathering product (smectite) is not rate-determining, the local chemical nano-environment immediately adjacent to smectite surfaces quite likely differs from the chemistry of more easily sampled pore fluids (Casey *et al.*, 1993; Hochella and Banfield, 1995). A thorough understanding of the influence of smectite porosity, permeability, and surface chemistry on the weathering of primary minerals depends on examining the weathering products, as well as mineral surfaces and textures, in the fully hydrated state. In addition, pyroxene and pyroxenites constitute a significant fraction of the known Martian mineralogy (McKay *et al.*, 1996; Fisk *et al.*, 2006). Evaluation of geological samples, whether remotely or on returned materials, for evidence of extraterrestrial life requires robust biosignatures developed from detailed knowledge of physical and biological pyroxene weathering processes, textures, and mineral relations.

Routine processing for scanning electron microscopy (SEM) analysis involves specimen dehydration, oftentimes resulting in images displaying drying artifacts due to tensional stresses during surface contraction. Critical point drying, another commonly used specimen-preparation technique, seeks to avoid surface tension artifacts through replacement of water by alcohol, which is in turn exchanged for liquid CO_2. The introduction of organic solvents may be problematical for smectites, because smectite textures are exquisitely sensitive to changes in the colloidal chemistry of their environment. This paper reports on the first use of high-pressure cryofixation (HPF) and cryo-field emission gun scanning electron microscopy (CryoFEG-SEM) on fully hydrated samples and examines the textures of smectite formed by natural weathering of pyroxene, emphasizing differences in textures that result from different sample-preparation methods.

MATERIALS

Naturally weathered pyroxene from clinopyroxenite of the Koua Bocca ultramafic intrusion was chosen for this study. Delvigne (1983, 1990, 1998) characterized exhaustively the weathering of this ultramafic body by fieldwork, optical petrography, and X-ray diffraction (XRD).

* E-mail address of corresponding author:
velbel@msu.edu
DOI: 10.1346/CCMN.2008.0560110

The Koua Bocca Precambrian ultramafic intrusive, located ~200 km NNW of Abidjan, Ivory Coast, western Africa, experienced contact metamorphism during the emplacement of a slightly younger Precambrian granite. Complex alteration of olivine and pyroxene produced a variety of hypogene and hydrothermal alteration products, including amphiboles and talc (Delvigne, 1983, 1990). Exposure and weathering inferred to be of Tertiary age produced deep residual/sedentary/relict lateritic regolith, superimposing weathering-derived mineral assemblages on the complex meta-ultramafic minerals (Delvigne, 1983, 1990). Both clino- and orthopyroxenes occur in the parent materials. The clinopyroxene (cpx) is diopsidic augite ($Wo_{45}En_{44}Fs_{11}$; Delvigne, 1983). The orthopyroxene (opx), which has been studied in somewhat greater detail, is bronzite, near hypersthene with a mean structural formula

$$Ca_{0.04}(Mg_{1.416}Fe_{0.506}Al_{0.024})(Si_{1.958}Al_{0.042})O_6$$

and trace octahedral Mn, Ti, and Cr (Delvigne, 1990). In any given weathered sample, the relative abundance of orthopyroxene is depleted relative to its abundance in the parent rock to a much greater degree than clinopyroxene, indicating that orthopyroxene weathers faster than clinopyroxene in the Koua Bocca regolith (Delvigne, 1983, 1998). Preferential weathering of orthopyroxene is evident in thin-section photomicrographs (*e.g.* Delvigne, 1998, photomicrographs 141 and 142) showing more extensive weathering of orthopyroxene grains immediately adjacent to less-extensively weathered clinopyroxenes. This is contrary to common experience elsewhere as well as to experimental augite and bronzite dissolution rates (Brantley and Chen, 1995; Brantley, 2005).

Ortho- and clinopyroxenes weather to clays and other secondary/tertiary minerals of various compositions, depending on the parent mineral, position in the landscape and regolith, and sampling depth (Delvigne, 1983, 1990). Product compositions depend on parent-mineral composition early in weathering and at greater depth, and on the extent of weathering/leaching later (Delvigne, 1983, 1990). The longest-exposed landscape surfaces are fersiallitic (kaolinite + gibbsite + ferruginous components) with some traces of bauxitic material. The youngest landscape surfaces have bisiallitic (smectite + vermiculite) regolith with calcareous and manganiferous concretions. Intermediate clay-mineral assemblages (smectite + kaolinite) with indurated ferruginous crusts characterize landscape surfaces of intermediate inferred exposure age. A similar sequence can be observed in weathering profiles and drill-cores, from ferrallitic at and near the surface, through fersiallitic at intermediate depths, to bisiallitic at the least-weathered depths (Delvigne, 1983, 1990).

The sample analyzed in this study thus represents a relatively young portion of the weathering profile, for both pyroxenes are replaced by compositionally similar low-charge (layer-charge deficiency ≈ 0.25 per $O_{10}(OH)_2$ formula unit) dioctahedral ferriferous nontronitic smectites (Delvigne, 1983, 1990). The structural formula for smectite formed from orthopyroxene (Delvigne, 1990, Table 1) is

$$Ca_{0.324}Mg_{0.117}K_{0.041}Na_{0.032}(Fe^{III}_{3.113}Mg_{0.514}Al_{0.313}Ti_{0.039}Mn_{0.011}Cr_{0.009})(Si_{7.535}Al_{0.465})O_{20}(OH)_4.$$

Delvigne (1983) reports that both orthopyroxene and clinopyroxene weather to very similar smectites which differ only slightly from true nontronite occurring in fractures. Smectite formed from clinopyroxene has ~3% less octahedral Fe, slightly less octahedral Mg, and slightly more octahedral Al and Ti than the smectite formed from orthopyroxene (Delvigne, 1983, Figure 1 and text).

The smectitic sample studied here comes from a depth of 2.8 m (Delvigne, pers. comm., 1992), immediately adjacent to depth intervals previously analyzed *via*

Table 1. Molar volume calculations.

Reactant-product pair	Element conserved	$n_{e,r}$ Per 6 O	V^o_p	$n_{e,p}$ Per 12 O	V^o_r	V_p/V_r
Clinopyroxene-expanded smectite	Si	2	219	3.768	66.039	1.76
	Fe	0.22	219	1.501	66.039	0.49
	Mg	0.88	219	0.275	66.039	10.6
Clinopyroxene-collapsed smectite	Si	2	128	3.768	66.039	1.03
	Fe	0.22	128	1.501	66.039	0.28
	Mg	0.88	128	0.275	66.039	6. 20
Orthopyroxene-expanded smectite	Si	1.96	219	3.77	62.676	1.82
	Fe	0.51	219	1.56	62.676	1.14
	Mg	1.42	219	0.32	62.676	15.7
Orthopyroxene-collapsed smectite	Si	1.96	128	3.77	62.676	1.06
	Fe	0.51	128	1.56	62.676	0.66
	Mg	1.42	128	0.32	62.676	9.17

https://doi.org/10.1346/CCMN.2008.0560110 Published online by Cambridge University Press

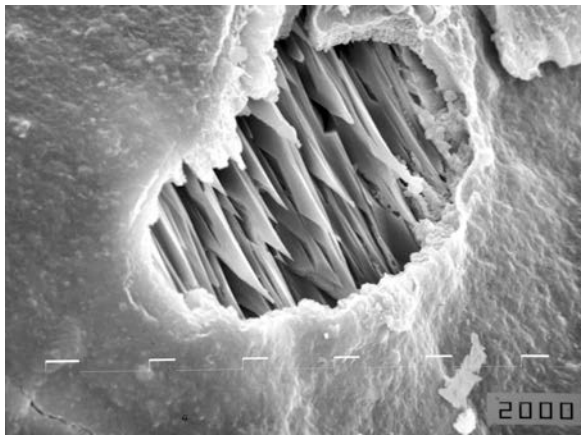

Figure 1. Denticulated cpx (~$Wo_{40}En_{41}Fs_{18}$ = augite) remnant with smectite. Note the absence of weathering products on denticles. Scale marks 10 μm apart. MSU JEOL T20 SEM.

petrographic thin-section photomicroscopy (Delvigne, 1983, 1998). Denticulated remnants of weathered orthopyroxene are partially replaced by smectite with a boxwork texture resembling classic meshwork serpentine, including the characteristic central parting (Delvigne, 1983, Plate B2; Delvigne, 1998, photomicrographs 132 and 133). Denticulated terminations of pyroxene remnants are easily visible in thin-section, as is the penetration of smectite between the denticles, giving the smectite at the interface a denticulated appearance that is the mold of the denticulated pyroxene margin (Delvigne, 1983, Plate B2; Delvigne, 1998, photomicrographs 132 and 133). Such molds are preserved even after removal of pyroxene remnants by dissolution (Delvigne, 1990) rather than by further replacement and oxidation and weathering of smectite (Delvigne, 1998, photomicrographs 377 and 378). Similar features of partially weathered orthopyroxenes and clinopyroxenes occur in other Koua Bocca samples (opx, Delvigne, 1998, photomicrographs 141 and 142: cpx, Delvigne, 1998, photomicrograph 056). Optical petrography results from Koua Bocca pyroxene and its weathering are consistent with pyroxene (and amphibole) weathering data from a number of previous studies (see review by Velbel, 2007). More advanced stages of weathering (*e.g.* complete pseudomorphism of smectite after pyroxene (Delvigne, 1983, Plates C1 and C2; and Delvigne, 1998, photomicrographs 292 and 293); dissolution of pyroxene remnants after partial replacement (Delvigne, 1998, photomicrographs 377 and 378)) were not examined in this study.

METHODS

Small chips of air-dried, partially weathered pyroxenite were glued to Al stubs, coated with Au, and examined using a JEOL T-20 SEM with a Polaroid camera in the Department of Geological Sciences at Michigan State University. Selected areas were re-examined with a JEOL 6400 SEM equipped with digital-image acquisition and a Noran energy dispersive spectroscopy (EDS) system at the Center for Advanced Microscopy at Michigan State University. Other samples were sputter coated at room temperature with Au and examined at 2.0 and 3.0 kV in a LEO FEG -SEM (Field-Emission Gun-Scanning Electron Microscope) at the University of Wisconsin – Madison. Confirmation of pyroxene compositions by EDS was not possible at the low operating voltages used for FEG-SEM. All FEG-SEM images were recorded digitally. Ultrarapid cryofixation, an alternate specimen-preparation technique to dehydration for SEM observation, produces vitreous ice and arrests the sample in a state most closely resembling the natural condition. In addition to elimination of surface-tension forces, cryofixation involves no change to the colloidal chemistry of the sample environment and thus is particularly well suited to the study of hydrated clay minerals as well as the structural and chemical relationships between natural clay surfaces and microbial components. High-pressure freezing (HPF) is the method of choice to cryo-immobilize relatively large specimens, up to depths of ~200 μm (Dahl and Staehelin, 1989). Specimens are sandwiched between metal holders ~2 mm in diameter. Two jets of room-temperature alcohol exert 2.1 kbar of pressure on the metal sample holder milliseconds prior to the freeze; two jets of liquid nitrogen flush out the alcohol maintaining the pressure during the freeze. The elevated pressure lowers the freezing point of water and reduces the rate of ice crystal nucleation and growth. Freezing is complete within 30 ms. Following cryofixation, ice present in the samples may be sublimed, exposing non-aqueous phases in the sample for study. By carefully controlling the sample pressure and temperature, ice sublimes or etches at a controlled rate. (This ice-sublimation process is referred to herein as freeze-etching, to distinguish it from the chemical corrosion process that produces etch pits and related features during natural and artificial weathering of chain silicates.) Following a suitable freeze-etching period, the now partially exposed but still frozen sample is cryo-metal coated for observations in the frozen hydrated state using a cryostage-equipped FEG-SEM.

Denticulated clinopyroxene grains with attached clay were hand-picked into gold planchets and rehydrated for 10 min with distilled water. Samples were high-pressure cryofixed in a Balzers HPM 010 high-pressure freezer using liquid nitrogen within 10 ms at 2.1 kbar, and freeze-etched and sputter-coated at −95ºC with 2 nm Cr using a Balzers Bal-Tec MED-010 Planar Magnetron Sputtering device modified for cryotechniques. Samples were held at −95ºC in a cryostage and digitally micrographed using an Hitachi S900 field emission high-resolution SEM operating at 1.5 kV. Selected anaglyph stereopairs, collected at 4º half angle, are

https://doi.org/10.1346/CCMN.2008.0560110 Published online by Cambridge University Press

available from the 'Deposited Material' section of journal pages on The Clay Minerals Society's website: www.clays.org/journal/JournalDeposits.html.

Product-reactant molar-volume ratios (V_p/V_r) were calculated for the replacement of Koua Bocca pyroxenes by smectite following the approach of Velbel (1993a, equation 2), who applied the Pilling-Bedworth relationship from metallurgy to silicate weathering. Assuming element *e* behaves conservatively during weathering (in other words, letting all of element *e* present in the reactant mineral be incorporated into the product mineral), the product-reactant volume ratio is given by $V_p/V_r = n_{e,r}V^o_p/n_{e,p}V^o_r$ where $n_{e,i}$ is the stoichiometric coefficient of element *e* in mineral *i*, and V^o_i is the molar volume of mineral *i* ($i = r$ for the reactant, p for the product).

V_p/V_r is the volume of product mineral produced per unit volume of reactant mineral, if element *e* is conserved. Previous applications of this concept to silicate-mineral weathering investigated the formation of transport-inhibiting ("protective") surface layers on Fe- and Al-bearing silicate minerals under well-leached, oxidizing conditions (Velbel, 1993a). Calculating the volume of product formed per unit volume of reactant consumed assumes conservative behavior of a minimally mobile element under the specific weathering conditions being investigated. If the volume of product formed is less than the volume of reactant consumed (in other words, if the product-reactant volume ratio is less than one), the product does not fully occupy the space left behind by the dissolving parent mineral (*e.g.* Delvigne, 1998). The resulting porosity allows easy diffusion of dissolved reactants and products to and from (respectively) the parent-mineral surface, such that solute transport through the product is not rate determining. If instead the product-reactant volume ratio is equal to (isovolumetric) or greater than one, the product is pseudomorphic (or alteromorphic in the terminology of Delvigne, 1998) and has no porosity. Solute diffusion through such products is much slower (grain-boundary diffusion, or diffusion through rather than around the product crystals) and potentially slow enough to control the rate of the overall weathering reaction. (For a more complete discussion of transport-limited destruction of primary minerals, see Velbel, 1993a and 2004.) In the case of expansible clay-mineral weathering products, interlamellar spaces function as nanopores and allow for diffusion to and from the reaction sites at the smectite-chain silicate interface. It remains to be established whether such interlayer diffusion can be slow enough to be rate determining for dissolution of primary rock-forming silicate minerals.

Elemental mobility during mineral weathering and replacement can also be investigated using this approach. If the volume of product is less than the volume predicted from the volume-ratio equation, then the element assumed to be immobile for the purposes of calculating the volume ratio has actually been mobilized (depleted) from the pseudomorph/alteromorph. If the volume of product is greater than predicted, then the element assumed to be immobile has been imported into the volume of the pseudomorph/alteromorph. Thus, comparing observed reactant-product volume relations with those calculated assuming immobility of individual elements allows inferences to be made regarding the actual mobility of those elements, at the scale of individual parent minerals and their pseudomorphic/alteromorphic weathering products.

The pyroxene-smectite reaction was chosen for this investigation because molar volume relations for pyroxenes altering to 2:1 phyllosilicates exceed the Pilling-Bedworth criterion (Velbel, 1993a) for isovolumetric replacement of reactant by product. Eggleton and Boland (1982) used transmission electron microscopy to observe textural and structural relations suggesting that enstatite weathers to talc. Assuming all Mg is conserved in the conversion of pyroxene to talc, and using stoichiometries and molar volumes of enstatite from Smyth and Bish (1988) and the method of Velbel (1993a), the volumetric product-to-reactant ratio for pyroxene weathering to talc is 1.45. This exceeds the Pilling-Bedworth threshold (unity) indicating that this reactant-product couple satisfies a minimum criterion for the product to act as a possible rate-determining protective surface layer (Velbel, 1993a). It also indicates that nearly one-third of the Mg in enstatite could actually be removed during alteration to talc and still result in isovolumetric replacement of enstatite by talc. These simple end-member calculations suggest that, unlike the common products of weathering in well-leached (ferrallitic, monosiallitic) weathering environments, which cannot form in sufficient abundance to form protective surface layers on common Fe-silicates such as amphiboles and pyroxenes (Velbel, 1993a), 2:1 phyllosilicates can form such volumetrically abundant and potentially diffusion-inhibiting products during bisiallitic weathering of pyroxene. The present study extends this approach to actual (rather than end-member) compositions of pyroxene and its bisiallitic weathering products (smectite).

To determine stoichiometric proportions of elements in Koua Bocca clinopyroxenes and their replacement products, clinopyroxene compositions reported by Delvigne (1983) and a smectite composition based on that of Delvigne (1990) were used. Molar volumes were selected from the literature to approximate the specific Koua Bocca minerals. The molar volume of diopside (66.039 cm^3/mol; table 6.2.1 from Smyth and Bish, 1988) was used to represent the molar volume of Koua Bocca clinopyroxene (diopsidic augite; Delvigne, 1983). The molar volume of pyrophyllite (128 cm^3/mol; table 7.1.1 from Smyth and Bish, 1988) was used as a proxy for fully collapsed dioctahedral phyllosilicate. A value of 219 cm^3/mol (between those of fully hydrated Na-saturated Upton and Chambers smectites; table 5 of

https://doi.org/10.1346/CCMN.2008.0560110 Published online by Cambridge University Press

Ransom and Helgeson, 1994) was used as a proxy for fully hydrated dioctahedral smectite. For comparison, similar calculations were made for Koua Bocca orthopyroxenes and their replacement products, using both compositions derived from Delvigne (1983) and more detailed updated analyses reported by Delvigne (1990). The molar volume of enstatite (62.676 cm^3/mol; table 6.1.1 from Smyth and Bish, 1988) was used to represent the molar volume of Koua Bocca orthopyroxene (bronzite, near hypersthene; Delvigne, 1983, 1990). The values used are shown in Table 1.

RESULTS

Conventional SEM

Conventional secondary electron images of air-dried samples show many instances of fine-grained material with a rolling topography, suggesting collapse of the fine-grained smectite onto the underlying pyroxene substrate. The clay surface, broken in numerous places, exposes denticulated pyroxene commonly devoid of directly adhering fine-grained reaction products. Elongate etch pits and denticulated terminations are common on partially weathered crystals and partially weathered remnants of fractured crystals, and appear visually identical to etch pits and denticles on naturally weathered chain silicates reported in numerous previous studies (*e.g.* Berner *et al.*, 1980; Berner and Schott, 1982; Nahon and Colin, 1982; Wilson, 1986; Velbel, 1989a; Colin *et al.*, 1990; Wilson, 2004; Wentworth *et al.*, 2005; Schaetzl *et al.*, 2006; see review by Velbel, 2007). Most examples of denticulated pyroxene are clinopyroxene (cpx). Delvigne (1983) reported that orthopyroxene (opx) weathers faster than cpx (unusual for px). Most opx in this sample from this depth in the regolith has extensively or completely weathered, leaving mostly partially reacted cpx for imaging. In conventional SEM, denticles on air-dried pyroxenes appear clean (free of visible products) in some instances (Figure 1), and in others, thinly coated by fine-grained, difficult-to-resolve material (Figure 2) occasionally exhibiting a 'cornflake' texture (Figure 2b). Some small denticulated pyroxene remnants exhibit doubly terminated remnants in single fields of view (Figure 3b, 3d).

Thin coatings on denticles are not the only clay texture visible in air-dried samples. Delvigne (1983, 1990, 1998) reported complete pseudomorphic and isovolumetric replacement of pyroxene by smectite from thin-section observations of other Koua Bocca samples. Smectite with boxwork or mesh-like textures (including central partings), commonly observed in thin sections (Delvigne, 1983, 1998), occurs in conventional SEM images of air-dried samples, almost invariably spatially associated with 'clean' denticles (Figure 3). As in thin section, peripheral voids separate denticulated remnants from the smectite boxwork. This indicates that an episode of isovolumetric replacement of pyroxene by smectite and boxwork formation is followed by destruction of pyroxene by dissolution. Continued dissolution of the parent mineral leaves void space between it and the earlier-formed clay, as has been reported from naturally weathered amphiboles by Proust *et al.* (2006). In some instances, masses of smectite appear to have pulled away by shrinkage from denticulated pyroxene margins (Figure 4), leaving a narrow but pervasive void between reactant and product phases (Figure 4). The formation of large voids at the smectite-pyroxene interface (an interface likely to resemble the amphibole-smectite interface examined in detail by Banfield and Barker, 1994) during air-drying implies that tensional forces, sufficient to disrupt this grain boundary, occur during natural hydration episodes. The change from a structurally coherent interface at nanometer scales to large voids may make possible significant change to the solute transport characteristics of the local weathering nano-environment.

Botryoidal masses of 'cornflake'-textured smectite directly associated with etched pyroxene surfaces

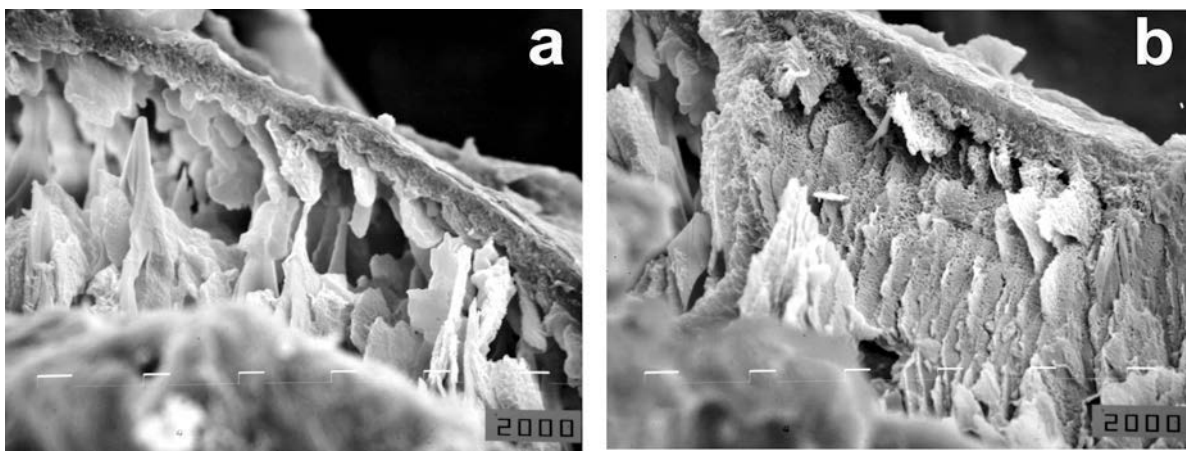

Figure 2. Denticulated termination covered with (collapsed?) smectite, and smectite marking original grain boundary (upper right). Note 'cornflake' texture characteristic of smectite in b. Scale marks 10 μm apart. MSU JEOL T20 SEM.

https://doi.org/10.1346/CCMN.2008.0560110 Published online by Cambridge University Press

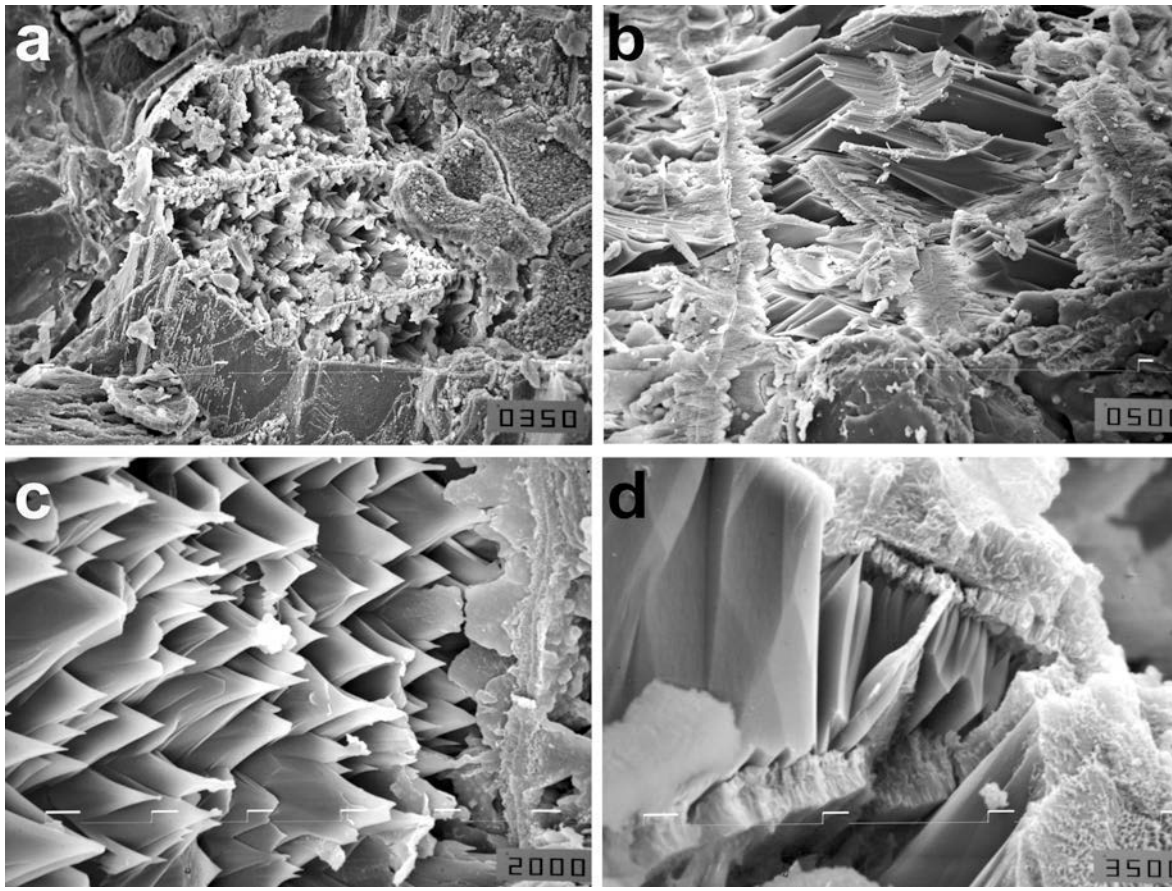

Figure 3. Denticulated pyroxene remnants associated with boxworks consisting of smectite in weathered pyroxenite. Delvigne (1998) presents color photomicrographs from petrographic thin sections illustrating identical features from near-identical depths in the same weathering profile. (a) Denticulated termination on cpx remnant (~$Wo_{42}En_{37}Fs_{22}$ = diopsidic augite), with boxwork. Scale marks 100 μm apart. (b) Doubly terminated denticulated opx (~$Wo_2En_{72}Fs_{25}$ = bronzite, near hypersthene) remnant with (early) peripheral replacement boxwork smectite with central parting, suggesting origin by replacement originating along trans-mineral fractures in weathered pyroxene. Scale marks are 100 μm apart. (c) Denticulated terminations on cpx (~$Wo_{46}En_{32}Fs_{22}$ = augite) and early peripheral replacement smectite boxwork with central parting. Note the absence of weathering products on denticles. Scale marks 10 μm apart. (d) Doubly terminated denticulated remnant on cpx (~$Wo_{34}En_{47}Fs_{19}$ = diopsidic augite) with smectite boxwork. Note the absence of weathering products on denticles. Scale marks 10 μm apart. MSU JEOL T20 SEM.

(Figure 5) suggest that some smectite forms by precipitation of dissolved products from solution, in addition to the smectite formed by direct replacement of pyroxene. The EDS of the 'cornflake'-textured material shows abundant Si, higher Fe and Al, and lower Ca and Mg, compared with EDS spectra of pyroxenes. This agrees with inferences from electron microprobe data by Delvigne (1983).

FEG-SEM

Air-dried samples. Air-dried pyroxene surfaces appear very smooth in FEG-SEM, and show many features similar to those observed in conventional SEM. These include elongate etch pits (Figure 6), doubly terminated pyroxene remnants with denticulated margins devoid of adhering products (Figure 7), denticles associated with products (Figure 8; a stereopair of the field of view in Figure 8 is available as Figure A1: www.clays.org/journal/JournalDeposits.html), and boxwork clays separated from denticulated pyroxene by large peripheral voids (Figure 9; a lower-magnification stereopair of the field of view in Figure 9 is available as Figure A2: www.clays.org/journal/JournalDeposits.html). Field-emission SEM reveals additional details of smectite texture not apparent from conventional SEM. Air-dried smectite boxworks consist of stacks of oriented wavy layers broadly perpendicular to grain boundaries of adjacent pyroxene remnants; the wavy layers commonly have vermiform edges (Figure 10; a lower-magnification stereopair of the field of view in Figure 10 is available as Figure A3: www.clays.org/journal/JournalDeposits.html). Similar vermiform edges occur on air-dried smectite filling etch pits (Figures 6, 11) and on thin edges of air-dried, denticulated margins (Figures 8, 12). 'Cornflake'-textured smectite occurs in etch pits or grooves in etched pyroxene (Figure 8; a stereopair of the field of view in Figure 8 is available as Figure A1) and at the tips of

https://doi.org/10.1346/CCMN.2008.0560110 Published online by Cambridge University Press

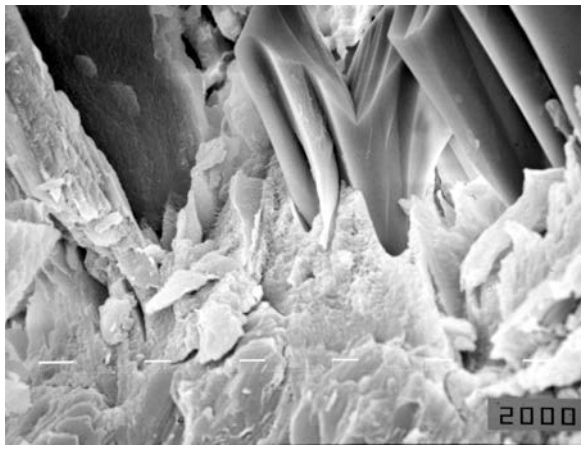

Figure 4. Denticles on small opx (~$Wo_2En_{64}Fs_{34}$ = bronzite, near hypersthene) remnants, covered with (collapsed replacement?) smectite. Note the product pulling away from the reactant, implying that the pyroxene-smectite interface is weak. Scale marks 10 μm apart. MSU JEOL T20 SEM.

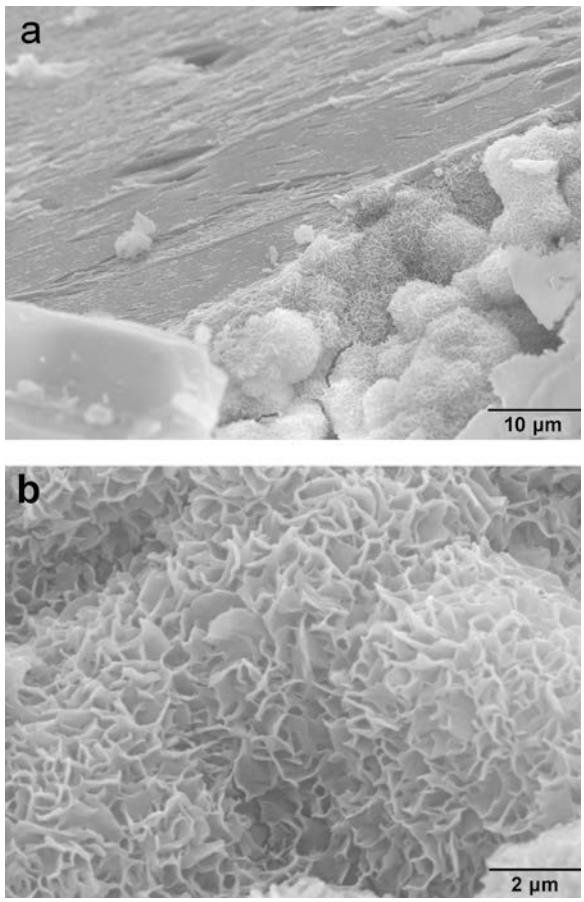

Figure 5. (a) Etched cpx (~$Wo_{38}En_{41}Fs_{21}$ = diopsidic augite) (top left background) with 'cornflake' smectite (neoformed?) bottom right foreground. (b) Closeup of 'cornflake' smectite. MSU CAM JEOL 6400 SEM.

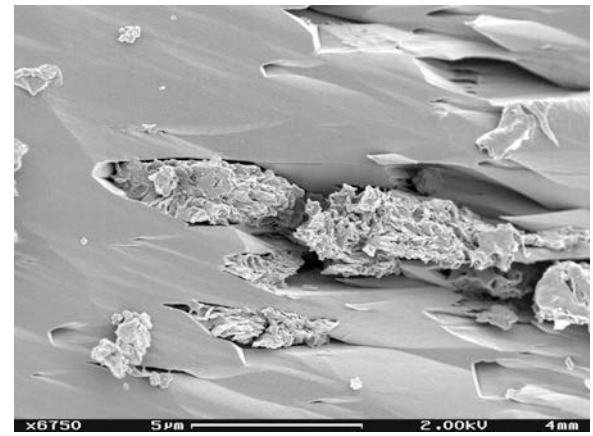

Figure 6. Incipient, crystallographically controlled, funnel-shaped and lenticular etch-pits, with smectite in all but the smallest pits. Air-dried sample. UW-M LEO FEG-SEM at 2.0 kV.

some denticles, the remainder of which are devoid of weathering products and often exhibit small crystallographically controlled grooves (Figure 13).

Freeze-etched samples. The HPF/freeze-etching eliminates surface-tension artifacts during partial sample drying *via* ice sublimation, and preserves the shape of microorganisms (Figure 14; a stereopair of this field of view is available as Figure A4: www.clays.org/journal/JournalDeposits.html) and extracellular polymers, suggesting that delicate textures of other naturally hydrous materials are similarly preserved. In contrast to large open pores seen in air-dried samples, CryoFEG-SEM of HPF samples reveals void-filling smectite in closer association with reaction-product-free pyroxene denticles displaying open cleavages (Figure 15). In other instances, small, flat lamellae, oriented parallel to the *c* axis, lend a distinct splintery appearance to pyroxene

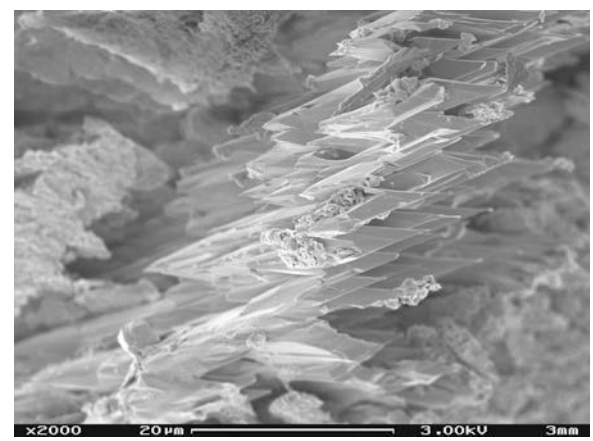

Figure 7. Doubly terminated denticulated pyroxene remnant, separated from smectite microboxwork by large peripheral void. Air-dried sample. UW-M LEO FEG-SEM at 3.0 kV.

https://doi.org/10.1346/CCMN.2008.0560110 Published online by Cambridge University Press

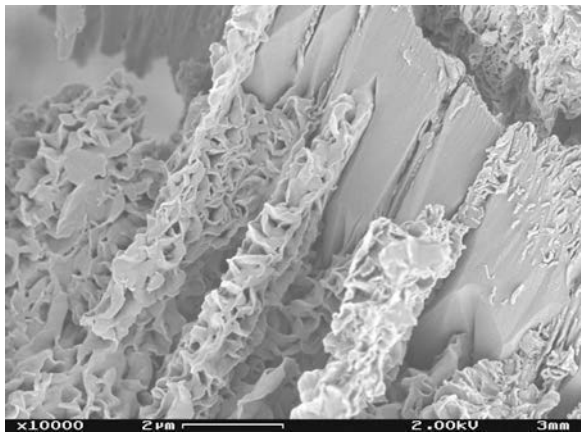

Figure 8. Denticulated remnant with attached 'cornflake'-textured smectite. Air-dried sample. UW-M LEO FEG-SEM at 2.0 kV. A stereopair of this field-of-view is available as Figure A1 (from the 'Deposited Material' section of journal pages on The Clay Minerals Society's website: www. clays.org/journal/JournalDeposits.html).

surfaces in fully hydrated samples (Figures 16, 17, 19). These lamellae often display a combination of straight (110) pyroxene edges and a crinkled border suggestive of smectite (Figures 18, 19). Narrow lenticular (110) open cleavages occur in both air-dried and HPF preparations and thus are not a pressurization artifact. Most often these openings contain no secondary minerals. Intergranular spaces between pyroxene denticles, lined with collapsed smectite in air-dried samples, are filled with thin packets of anhedral smectite crystallites oriented face to face when hydrated (Figure 18). Occasional regions of edge-to-face 'house of cards' texture also occur (Figure 19; a stereopair of the field of view in Figure 19 is available as Figure A5: www.clays.org/journal/JournalDeposits.html). Pores actually present during a weathering episode thus are smaller and more numerous than would be expected from examining air-dried materials.

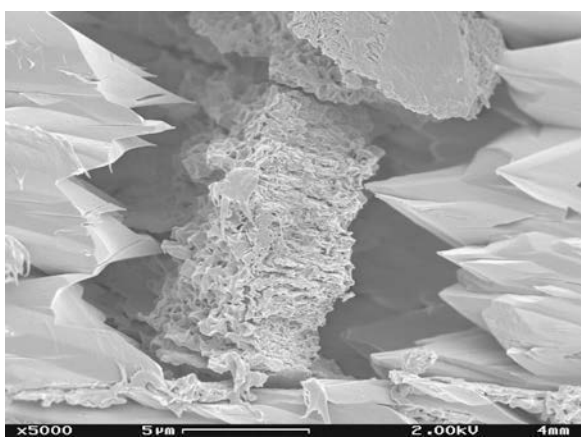

Figure 9. Smectite microboxwork separated from denticulated pyroxene by large pore spaces. Air-dried sample. UW-M LEO FEG-SEM at 2.0 kV. A lower-magnification stereopair of this field-of-view is available as Figure A2 (from the 'Deposited Material' section of journal pages on The Clay Minerals Society's website: www.clays.org/journal/JournalDeposits.html).

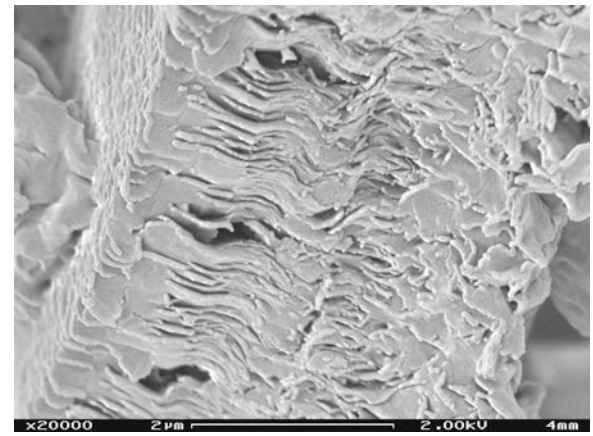

Figure 10. Higher-magnification view of smectite microboxwork showing imbricated arrays of face-to-face oriented layers with little interlamellar porosity. Air-dried sample. UW-M LEO FEG-SEM at 3.0 kV. A lower-magnification stereopair of this field-of-view is available as Figure A3 (from the 'Deposited Material' section of journal pages on The Clay Minerals Society's website: www.clays.org/journal/JournalDeposits.html).

Reactant-product molar volume relations

Using published compositional data for Koua Bocca clinopyroxene, orthopyroxene, and their weathering products, and using published molar volumes from compositionally similar pyroxenes and smectites, specific (rather than idealized) reactant-product molar-volume relationships have been calculated for Koua Bocca pyroxenes and their weathering products (Table 1). Using the stoichiometries described in the introduction and the molar volumes described in the

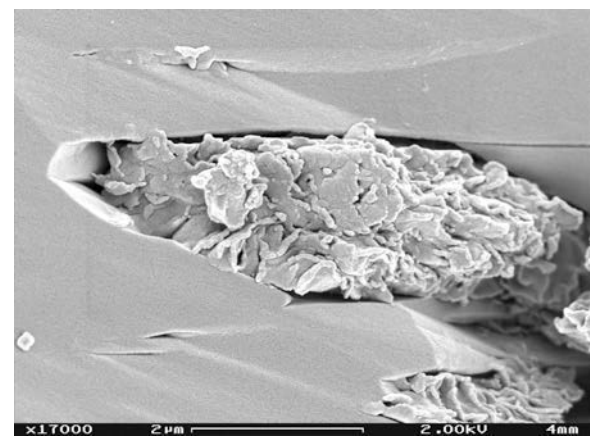

Figure 11. Close-up of Figure 6, showing smectite in a larger lenticular etch-pit. Note the presence of open cleavages which control the location of the etch pits. Air-dried sample. UW-M LEO FEG-SEM at 2.0 kV.

https://doi.org/10.1346/CCMN.2008.0560110 Published online by Cambridge University Press

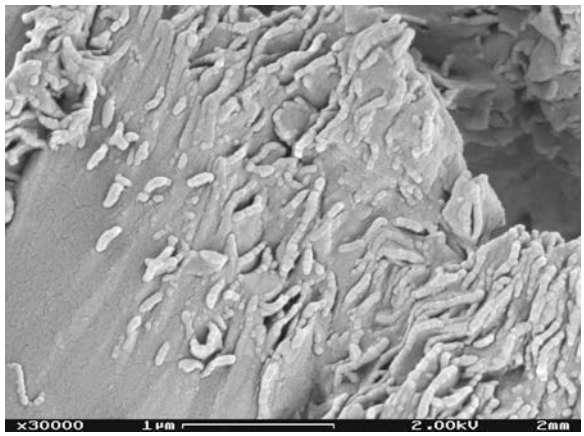

Figure 12. Close-up of right edge of Figure 8, showing the edge of a pyroxene remnant with wavy smectite and vermiform structures resulting from Au sputter coating on clay crystallite edge faces. Air-dried sample. UW-M LEO FEG-SEM at 2.0 kV.

methods section, product-reactant volume ratios (V_p/V_r) were calculated for each Koua Bocca pyroxene weathering to its specific smectite product. For each reactant-product pair, V_p/V_r was computed assuming conservative behavior of Si, Fe, or Mg (each assumption resulting in a different V_p/V_r). Each such computation was performed twice, once using a pyrophyllite molar volume to represent the minimum (collapsed) volume of 2:1 phyllosilicate product that would be produced from a unit volume of reactant pyroxene assuming conservation of a given element, and again using a smectite molar volume to represent the maximum (hydrated, expanded) volume of product that could be formed, all other assumptions being equal. The values used, and the results, are shown in Table 1. Although the composition of smectite formed from clinopyroxene is not as well constrained as that formed from orthopyroxene (above), calculations using slightly different stoichiometry for smectite formed from clinopyroxene give results similar to within 5% of the value reported in Table 1.

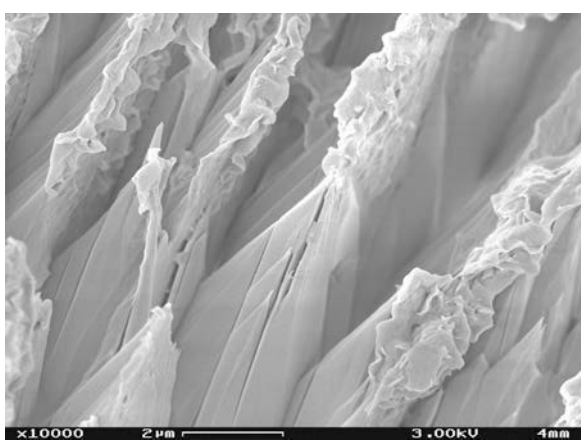

Figure 13. Denticulated termination with smectite at some tips. Note open cleavages which define one denticulation edge. Air-dried sample. UW-M LEO FEG-SEM at 3.0 kV.

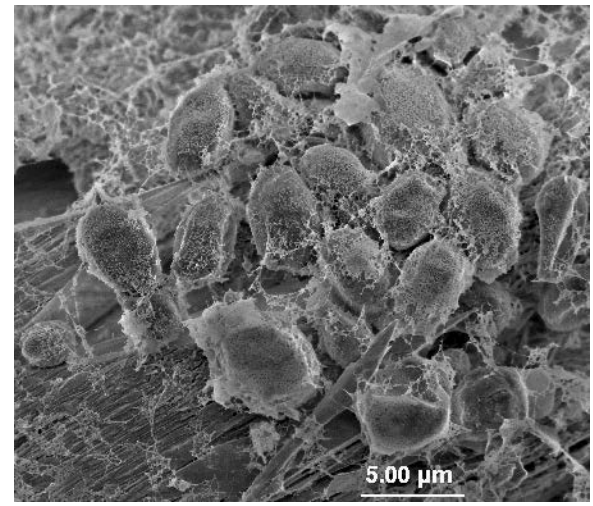

Figure 14. Biofilm covering denticulated pyroxene. Note detailed preservation of texture of biofilm (microbial community and extracellular polysaccharides). HPF/freeze-etched sample. UW-M Hitachi S900 FEG-SEM at 1.5 kV. A stereopair of this field-of-view is available as Figure A4 (from the 'Deposited Material' section of journal pages on The Clay Minerals Society's website: www.clays.org/journal/JournalDeposits.html).

For Koua Bocca pyroxenes, replacement by fully collapsed 2:1 phyllosilicate is essentially isovolumetric (V_p/V_r = 1.0) if Si is conserved (V_p/V_r = 1.03 for cpx, 1.06 for opx). This is consistent with the widely accepted mechanism by which tetrahedral chains in pyroxene are rearranged into the tetrahedral sheets of 2:1 layer-

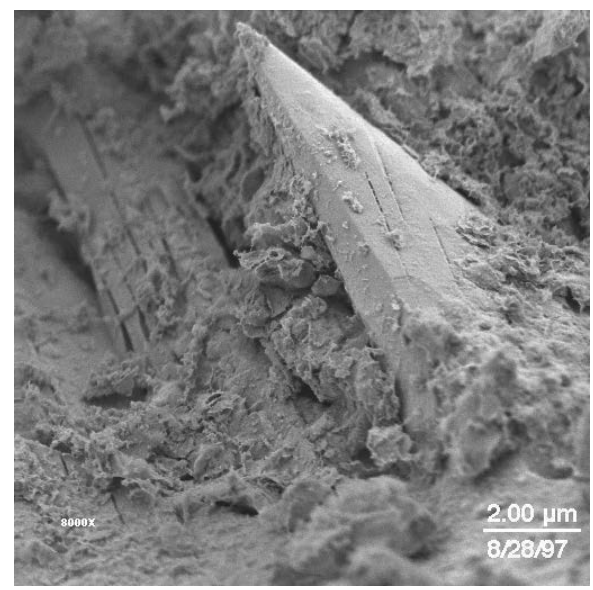

Figure 15. Denticulated termination. Note the absence of large open pores seen in air-dried samples. HPF/freeze-etched sample. UW-M Hitachi S900 FEG-SEM at 1.5 kV.

https://doi.org/10.1346/CCMN.2008.0560110 Published online by Cambridge University Press

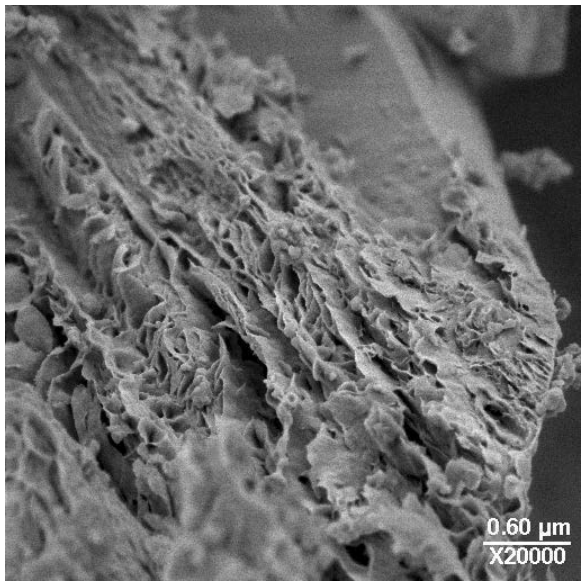

Figure 16. Denticulated pyroxene remnant with 'cornflake' textured smectite. Note the topotactic relationship apparent between reactant and product minerals, as well as nanoporosity apparent in the hydrated interlamellar spaces. HPF/freeze-etched sample. UW-M Hitachi S900 FEG-SEM at 1.5 kV.

structured weathering products (*e.g.* Eggleton, 1975), resulting in volume-for-volume replacement of pyroxene by smectite and pseudomorphism of pyroxene by smectite. This phenomenon has been observed at unit-cell scales (by transmission electron microscopy, TEM) for alteration of chain-silicates to 2:1 phyllosilicates

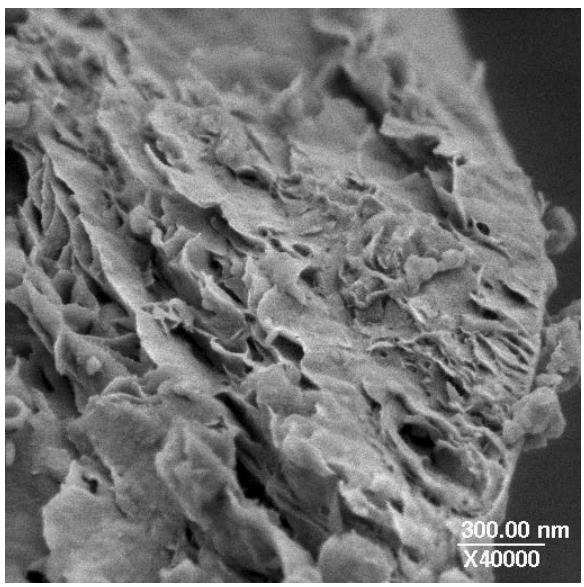

Figure 17. Detail of Figure 16 illustrating nanoporosity at the reactant-product interface. Denticulated pyroxene remnant with 'cornflake'-textured smectite. HPF/freeze-etched sample. UW-M Hitachi S900 FEG-SEM at 1.5 kV.

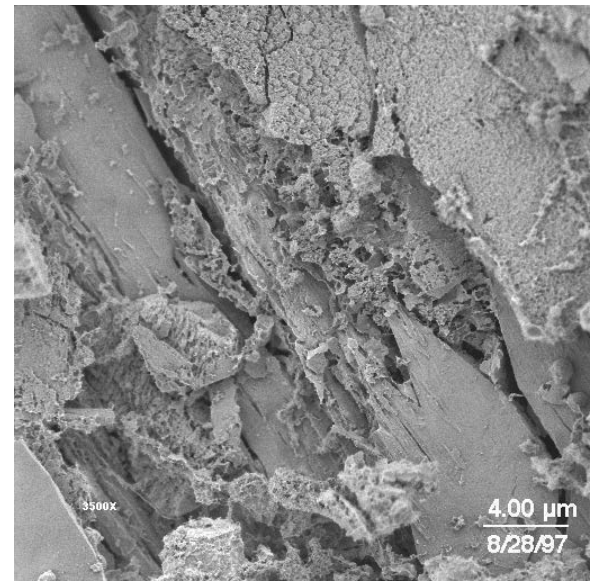

Figure 18. Denticulated pyroxene termination with spongy porous smectite. Large open pore spaces seen in air-dried samples are filled with expansible smectite in these hydrated samples. HPF/freeze-etched sample. UW-M Hitachi S900 FEG-SEM at 1.5 kV.

during aqueous alteration; examples include pyroxene altering to talc (Eggleton and Boland, 1982) and amphibole weathering to smectite (Banfield and

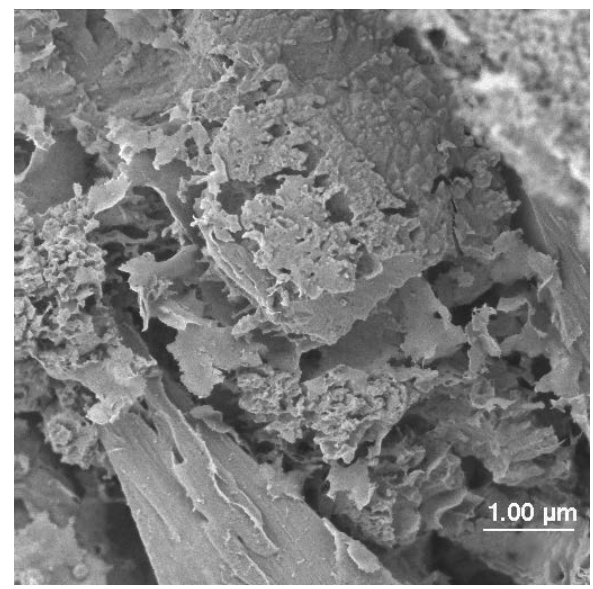

Figure 19. Detail of Figure 18 showing denticulated termination with spongy porous smectite. In contrast to the smooth surfaces seen on air-dried samples, note the 'tube' and partially detached, wavy smectite on a denticle in the lower left. HPF/freeze-etched sample. UW-M Hitachi S900 FEG-SEM at 1.5 kV. A stereopair of this field-of-view is available as Figure A5 (from the 'Deposited Material' section of journal pages on The Clay Minerals Society's website: www.clays.org/journal/JournalDeposits.html).

https://doi.org/10.1346/CCMN.2008.0560110 Published online by Cambridge University Press

Barker, 1994). This suggests that weathering of pyroxene to smectite at Koua Bocca is consistent with mechanisms of pyroxene (and amphibole) weathering elsewhere, and further that the assumptions invoked in using the structural formulae from the published data of Delvigne (1983, 1990) and those introduced through the use of molar volumes from proxy minerals in the molar volume calculations have not introduced substantial error into the results. Molar-volume calculations invoking hydrated (rather than fully collapsed) smectite indicate that larger volumes of hydrated smectite can be formed if Si is conserved, and/or that some Si can behave non-conservatively (be removed in solution) and still result in formation of a mass of weathering product that is isovolumetric relative to the parent pyroxene.

DISCUSSION

Relative persistence of different pyroxenes to natural weathering

Berner and Schott (1982) observed that augite weathers preferentially relative to hypersthene in a compound soil grain comprising discrete crystals of both pyroxenes. Subsequently, Berner and Berner (1996) inferred that this difference in susceptibility to weathering is due to presumed higher dislocation density in augite than in hypersthene. Other work has suggested compositional rather than structural influence. Laboratory experiments suggest that diopside dissolves faster than enstatite (Schott *et al.*, 1981) and bronzite (Schott and Berner, 1983) over a broad range of experimental acidic pH conditions, and augite is more extensively corroded than immediately adjacent hypersthene in natural soil (Berner and Schott, 1982). These observations suggest that calcic pyroxenes weather faster than Ca-poor pyroxenes. However, in other occurrences, observations do not support such simple composition/susceptibility relationships. In saprolite developed on mafic-ultramafic rocks of the Koua Bocca Complex, the relative abundance of orthopyroxene (bronzite) is depleted relative to its abundance in the parent rock to a much greater degree than clinopyroxene (diopsidic augite), indicating that, contrary to experience elsewhere in both experimentally and naturally weathered materials, orthopyroxene weathers faster than clinopyroxene in the Koua Bocca regolith (Delvigne, 1983, 1998). A compilation and review of experimental pyroxene dissolution rates (Brantley and Chen, 1995) shows that dissolution rates at pH = 2 decrease in the sequence augite > enstatite > diopside > bronzite; because the dissolution rates for different pyroxenes have different pH dependences, the sequence of relative dissolution rates at pH = 5 is enstatite > diopside > augite = bronzite (Brantley and Chen, 1995, fig. 10). Extrapolating slightly from the compilation of Brantley and Chen (1995, fig. 10), bronzite dissolves faster than augite at pH > 5. The observed relative persistence of these two pyroxenes in the Koua Bocca weathering profiles (Delvigne, 1983, 1998) may be consistent with the relative persistence of the same minerals implied by the compiled experimental dissolution rates (Brantley and Chen, 1995), if the Koua Bocca pyroxenes were weathered at high pH.

Velbel (1993b) showed that interlaboratory variations can obscure some trends in experimentally determined relative dissolution rates of silicate minerals, and showed how clearer relationships are apparent when rates for inter-mineral comparisons are selected only from those produced by the same laboratory. Experimentally determined dissolution rates for diopside are greater than for bronzite over the entire range of pH conditions (pH = 6) examined by Schott *et al.* (1981) and Schott and Berner (1983), but the rates are more similar at pH = 6 than at more acidic pHs. If the rates become equal at higher pH, there may be a pH above which bronzite weathers faster than diopside. This would be consistent with the observed relative persistence of Koua Bocca pyroxenes, if they weathered at high pH as suggested above. Such pHs would be consistent with the formation of smectite as the weathering product of pyroxenes at Koua Bocca (Delvigne, 1983, 1990, 1998). Experimental studies of pyroxene dissolution kinetics (like those summarized by Brantley and Chen, 1995) need to be extended to higher pHs.

Textures of clay minerals formed by pyroxene weathering, and implications

Evidence from optical petrography indicates that the smectite front closely mimics the denticulated (retreating) pyroxene surface during early stages of pyroxene weathering to smectite; at later stages, continued removal of pyroxene produces void space bounded by the retreating parent mineral and the smectite 'cast' of the former denticulated pyroxene-smectite contact (Delvigne, 1983, 1990). Observations by SEM of weathered amphiboles (Proust *et al.*, 2006) show that smectites are initially in contact with flat amphibole surfaces ((001) or (110)). Continued weathering causes denticle formation on the amphibole (001) surface while smectites remain in contact with the tips of denticles. Void space between amphibole and smectite in this instance is created by dissolution.

Both conventional SEM and FEG-SEM images of some air-dried samples show void space around what appear to be clay-coated denticles (Figures 2, 9; a lower-magnification stereopair of the field of view in Figure 9 is available as Figure A2). Some FEG-SEM images of air-dried samples show preferential association of smectite with the tips of otherwise clay-free denticles (Figure 13). Conventional and FEG-SEM images of other air-dried samples show a gap between smectite and pyroxene (*e.g.* Figures 4, 6, 11) or what appear to be clay-free denticles separated from oriented clay boxworks by larger distances (Figures 1, 3, 7, 9; a lower-

https://doi.org/10.1346/CCMN.2008.0560110 Published online by Cambridge University Press

magnification stereopair of the field of view in Figure 9 is available as Figure A2), indicating separation of smectite from denticles by volumetric change of the smectite and/or continued dissolution of pyroxene after cessation of smectite formation. Cryo-FEG-SEM images of HPF/freeze-etched samples clearly show interlamellar nanoporosity present in fully hydrated smectite samples (Figures 16, 17). These interlamellar spaces allow for fluid access to the reaction front during the isovolumetric stage of pyroxene to smectite transformation. Cryomicroscopy also indicates that clay-free denticles (Figure 15) and denticles partially or completely surrounded by clay in contact with the denticulated pyroxene (Figures 16–19) both occur in this single sample. When present, distinct peripheral voids separating pyroxene denticles from nearby smectite are much smaller in HPF/freeze-etched preparations (Figures 15–19; a stereopair of the field of view in Figure 19 is available as Figure A5) than in air-dried preparations. Cryomicroscopy of these fully hydrated samples (Figures 18, 19) also reveals that many denticles that appear smooth in air-dried preparations may in reality be a smectite surface. Thus, while dehydration and shrinkage of the smectite results in larger pore-void formation near the pyroxene-smectite interface, these pores are smaller and in part occupied by hydrated smectite during a hydration event. Improved fluid access to reaction sites initiates extensive dissolution of pyroxene resulting in clay microboxworks increasingly isolated by ever enlarging voids from the retreating, dissolving, denticulated pyroxene surface. This explains optical petrographic and SEM imagery of more advanced stages of weathering showing continued chain-silicate dissolution after cessation of clay formation (Delvigne, 1983, 1998; Velbel, 1989; Proust *et al.*, 2006).

Smectite formed by weathering of pyroxene (or amphibole) is crystallographically and structurally continuous with the parent mineral across the pyroxene–smectite (or amphibole–smectite) interface (Eggleton, 1975; Cole and Lancucki, 1976; Delvigne, 1983, 1990; Banfield and Barker, 1994). Smectite experiences volume change during natural moisture fluctuations and during dehydration associated with sample preparation. All such volume change occurs within the smectite on one side of the pyroxene–smectite interface; no similar changes occur in the primary silicate parent mineral. In bulk smectite, far from the interface, such volume change is unconstrained. However, near the coherent chain-silicate–smectite interface, smectite layer edges are continuous with and fixed to the parent mineral structure. Volume change in smectite far from the interface presumably produces associated tensional and flexural stresses and structural fatigue at or very near the interface between the material that changes volume (the smectite) and the material that does not (the parent pyroxene or amphibole). The parting about which pyroxene and smectite are seen to separate in the SEM images of this study probably develops in response to this structural fatigue.

Whether the tensional/flexural stresses associated with hydration/dehydration cycles cause separation at the interface itself or at some point a few unit cells into the smectite (leaving a few unit cells of smectite attached to the pyroxene) remains to be established. Our FEG-SEM images suggest that both phenomena may occur in different portions of the same sample. Volume change during hydration/dehydration cycling of smectite is largely uniaxial (expansion and contraction of the smectite interlayer region, resulting in dimensional change perpendicular to the smectite 2:1 layers). Where smectite layers 'onlap' onto the pyroxene structure along the flanks of denticles, changes in interlayer volume can pry the smectite away from the pyroxene; this leaves denticles with thin broken smectite edges (*e.g.* Figure 12) or entirely without adhering clay. Dimensional change within the layers themselves is minimal, so flexural or tensional stresses in directions parallel to the 2:1 layers are likewise minimal. Phyllosilicate oriented such that its 2:1 layers cannot be flexed from the pyroxene (*e.g.* at the tips of denticles; Figure 13) remains preferentially attached.

Field-emission SEM reveals important differences in different preparations of otherwise identical smectite samples. Vermiform edges of wavy smectite layers appear only in Au sputter-coated, air-dried samples (Figures 8, 10–12; stereopairs corresponding to Figures 8 and 10 are available as Figures A1 and A3, respectively: www.clays.org/journal/JournalDeposits.html). Such features are absent from the edges of porous, 'cornflake', 'cobweb', or crinkled smectite in freeze-etched samples (Figures 15–19), suggesting they are a sample preparation artifact attributable to metal sputtering and specific to smectite edges in air-dried samples. The various smectite morphologies preserved in air-dried samples occupy only a fraction of the volume vacated by the destruction of the parent mineral (pyroxene).

The preservation of greater detail and more natural, hydrated textures made possible by cryoFEG-SEM of HPF/freeze-etched samples of smectite formed by natural weathering will help inform and solve a long-standing problem in the study of the geochemical kinetics of silicate weathering reactions. It has been known for the past several decades that silicate-mineral weathering rates determined from natural systems (by a variety of means) are up to three orders of magnitude slower than rates determined experimentally in the laboratory (Pačes, 1983; Velbel, 1985, 1986, 1989b, 1990, 1993b; Bowser and Jones, 2002; White and Brantley, 2003; Bricker *et al.*, 2005; Brantley, 2005). Among the many causes proposed for this phenomenon, some experimental work on feldspars (Nugent *et al.*, 1998) and on whole soils with heavy-mineral fraction dominated by amphibole (Courchesne *et al.*, 1996) has suggested that natural coatings (rich in the relatively

https://doi.org/10.1346/CCMN.2008.0560110 Published online by Cambridge University Press

least-mobile major elements, *e.g.* Fe and Al) on primary minerals in nature suppress the rates of weathering of, and elemental release from, the underlying primary minerals. Most geochemical rate laws for silicate dissolution indicate that rates slow down drastically as the concentration of dissolved weathering products increases. While natural soil solutions (that often move rapidly to sampling sites through macropores; Velbel, 1993b) are often too dilute to be in the range where solute concentration suppresses reactant dissolution rate (*e.g.* Velbel, 1989b), much less is known about chemical conditions in closed weathering microsystems with hard-to-sample micropores.

Molar-volume ratios for smectite formed by transformation from Koua Bocca pyroxenes suggest that low porosity should be expected in the weathering products. As noted above, if Si is conserved during pyroxene replacement, the replacement of both clinopyroxene and orthopyroxene by fully collapsed (dehydrated) smectite is isovolumetric (Table 1). This is consistent with structural inferences (Eggleton, 1975; Cole and Lancucki, 1976) and TEM observations (Eggleton and Boland, 1982; Banfield and Barker, 1994) that: (1) the silicate tetrahedra of the primary mineral become the silicate tetrahedra of the alteration product without significant compositional change; and (2) the x axis repeat spacing of I beams in chain silicates controls the z axis repeat distance between successive sheets in the 2:1 phyllosilicates that replace chain silicates. The fully collapsed nature of 2:1 phyllosilicates formed by direct replacement of chain silicates during weathering implied by the volumetric calculations and observed by TEM suggests that the initial weathering of a chain silicate to a 2:1 phyllosilicate does not require immediate hydration of an interlayer cation.

The initial formation of fully dehydrated smectite is followed on some time scale by hydration of the interlayer cation and consequent expansion of the smectite. If expansion coincides in time with loss of ions from the smectite, Si loss can occur while maintaining isovolumetric weathering by formation of more fully hydrated smectite. Volumetric calculations indicate that the product volume exceeds reactant volume if Si is conserved and the product is hydrated, by as much as 76% if the product is fully hydrated (Table 1). Mobilization (loss) of some of the Si and formation of partially or fully hydrated smectite eventually occur in this (or any) natural weathering system, but may only occur after an initial step of isovolumetric replacement of primary chain silicate by dehydrated 2:1 phyllosilicate. After such initial isovolumetric replacement, some Si is lost to solution (rather than conserved), accompanied by formation of a volume of hydrated smectite equal to or greater than the volume of pyroxene weathered.

Mobilization of additional Fe over and above that available from the clinopyroxene is required to form the full smectite volume possible from Si conservation; even assuming a maximum molar volume for fully hydrated smectite, Koua Bocca clinopyroxene contains only half the Fe required to form an equal volume of smectite of the observed composition (Table 1). For the clinopyroxene-smectite replacement to be isovolumetric (or form $V_p/V_r > 1$), Fe must be imported to the pseudomorph to form smectite of the observed composition. Koua Bocca clinopyroxene does not contain enough Fe to form smectite of the observed composition from the constituents of clinopyroxene alone. However, Fe-rich orthopyroxene weathers faster than clinopyroxene at Koua Bocca (Delvigne, 1983, 1990) and contains more Fe than required to form an equal volume of smectite if partially or fully hydrated smectite is assumed (Table 1). Rapid weathering of olivine (which also occurs in this profile) could also supply Fe to the weathering products of clinopyroxene. Consequently, the faster weathering of, and import of Fe from, orthopyroxene and/or olivine may be the source of the additional Fe required for the formation of the full amount of smectite possible from Si conservation during clinopyroxene weathering. Alternatively, pyroxene replacement by smectite may not be isovolumetric. If Fe is regarded as an immobile element, clinopyroxene contains only enough Fe to form a volume of smectite (of the observed composition) less than half that required for isovolumetric weathering. If Fe is conserved, a high-porosity mass of smectite forms, and much Si is removed in dissolved form from the porous pseudomorph. Although both phenomena (isovolumetric weathering of pyroxene to smectite, and formation of porous alteromorphs during weathering) are observed, the latter are common only at more advanced stages of pyroxene weathering at Koua Bocca (Delvigne, 1983, 1990, 1998). Whether clinopyroxene replacement is isovolumetric (as at early stages, forming low-porosity boxworks of smectite) or forms a porous pseudomorph (at later stages), the resulting weathering product has abundant internal nano- and microporosity. Smectite-surface chemistry in such small pore spaces probably influences the chemistry of the aqueous medium immediately surrounding the dissolving pyroxene (Casey *et al.*, 1993; Hochella and Banfield, 1995).

Magnesium is clearly present in both pyroxenes in abundances well in excess of the amount of Mg required to form isovolumetric smectite, regardless of the hydration state assumed, consistent with export of Mg during weathering. Clinopyroxene is still present even after near-complete removal of orthopyroxene (Delvigne, 1983). The formation of smectite with nearly identical composition (probably including small interlayer Ca abundances) to that formed from orthopyroxene indicates that Ca is largely removed from the weathering profile during late-stage clinopyroxene weathering (Delvigne, 1983). The presence of interlayer Ca in smectite formed from orthopyroxene (Delvigne, 1990) indicates some within-profile transfer of Ca from parent

clinopyroxene to the product of orthopyroxene (*e.g.* Nahon, 1991). Smectite formed from orthopyroxene has considerably more Al than could be derived from the parent orthopyroxene (Delvigne, 1990), suggesting import of Al from some other mineral source (local or up-profile). Too little is known about the minor abundance of Al in the parent clinopyroxene and the product smectite for either reliable molar-volume calculations or inferences about the mobilization of the small amount of Al to be expected in clinopyroxene.

If HPF/freeze-etching preserves natural, hydrated smectite textures better than air-drying, pore spaces in smectite formed by natural weathering are more numerous and smaller than appears the case from examination of air-dried samples. Diffusion pathways through the small pores imaged from freeze-etched smectite are probably much more tortuous than is the case for the large, continuous pores imaged at similar and (more commonly) lower magnifications from air-dried samples. Furthermore, the much greater internal surface area of smectite within masses with small pores will probably result in the smectite's surface chemistry exerting a much stronger influence on pore fluids in the micropores than would be the case for larger more continuous pores inferred from imagery of air-dried samples. Thus, even if diffusion through small pores in smectite is not rate limiting, the smectite may dominate solution chemistry in the immediate vicinity of the adjacent pyroxene surface undergoing weathering; the chemistry of pore solutions in these microenvironments may be considerably different from the chemistry of weathering solutions in larger pores that would be better connected to fast-flowing soil solutions (Casey *et al.*, 1993; Hochella and Banfield, 1995). The chemistry of micropore solutions near abundant smectite surface may be significantly more concentrated than bulk macropore fluids; if so, the effect may be to suppress the dissolution rate relative to that expected from dilute macropore solutions.

CONCLUSIONS

High-magnification imaging of pyroxene denticles in air-dried samples using field-emission secondary electron imaging reveals a range of fine-scale surface textures only hinted at in conventional SEM images. Denticles on air-dried pyroxenes imaged with FEG-SEM appear clean in some instances, and thinly coated with vermiform or wispy textured products on others. Pyroxene denticles in HPF/freeze-etched samples imaged with FEG-SEM are thinly coated with 'cobweb'- or 'cornflake'-textured products, some of which partly fill small-scale etch pits on the larger denticles.

The appearance of smectite formed by pyroxene weathering varies with sample preparation. In air-dried sample mounts, smectite with boxwork or mesh-like textures is visibly separated from denticles (apparently by shrinkage) in conventional SEM images of air-dried samples. Boxworks are separated from denticulated remnants by large empty peripheral voids in conventional and FEG-SEM images of air-dried preparations. As imaged with field-emission SEM, air-dried smectite boxworks are separated from denticulated remnants by large peripheral voids and consist of stacks of wavy oriented layers broadly parallel to denticles on adjacent pyroxene remnants; the wavy layers commonly have vermiform edges. In contrast, weathering products appear porous, wispy, and variously 'cobweb'- or 'cornflake'-like in FEG-SEM images of freeze-etched preparations. Unlike the large, continuous pores that appear in air-etched samples, due to shrinkage of smectite and consequent pulling away of the smectite from the denticulated pyroxene-smectite interface, pore space seen in freeze-etched samples is much smaller in scale. Thus, based on these observations, we propose a multistage model for pyroxene weathering to smectite. Ingress of water along open grain boundaries and sprung cleavages initiate topotactic, isovolumetric reactions. At some point, oriented clay boxwork layers become susceptible to mechanical disruption, probably by episodic surface tension forces of water during natural wet and dry cycles. Once a rupture forms at or near the smectite-pyroxene interface, improved fluid access favors solute transport and more complete dissolution of pyroxene. The extent to which nearby smectite layers serve as templates for continued clay formation or whether dissolved constituents are transported away from reaction sites to recrystallize elsewhere remains an open question. At some point porosity increases sufficiently to allow colonization of pore spaces by microbial colonies, ushering in a final weathering stage in which microbes and their extracellular polymers create and control a diverse suite of physiochemical nano-environments. Resulting microboxwork textures known from pyroxene and amphibole-derived saprolites constitute the end product of this process. Improved insight into the microtextures of naturally formed clay minerals made possible by improved sample-preparation methods may shed new light on the role of clays, their microtextures, and the chemical microenvironments the microtextures produce on reactions and rate processes of importance in environmental biogeochemistry and global geochemical cycling.

ACKNOWLEDGMENTS

We are grateful to our colleagues Y. Chen (cryomicroscopy), C.A. Lavin (cryofixation), and J.F. Banfield (data analysis). Ewa Danielewicz (Michigan State University Center for Advanced Microscopy) assisted with acquisition of EDS data. Reviews by D. Proust and an anonymous reviewer were helpful and are appreciated. This research was supported by a grant from the Michigan State University Office of International Studies and Programs (MAV), NSF Grant CHE9714014 (WWB), and NASA Grant NNG05GL77G (MAV).

We dedicate this paper to the memory of Jean Delvigne.

REFERENCES

Banfield, J.F. and Barker, W.W. (1994) Direct observation of reactant-product interfaces formed in natural weathering of exsolved, defective amphibole to smectite; evidence for episodic, isovolumetric reactions involving structural inheritance. *Geochimica et Cosmochimica Acta*, **58**, 1419–1429.

Berner, E.K. and Berner, R.A. (1996) *Global Environment: Water, Air, and Geochemical Cycles*. Prentice-Hall, Englewood Cliffs, New Jersey, USA.

Berner, R.A. and Schott, J. (1982) Mechanism of pyroxene and amphibole weathering – II. Observations of soil grains. *American Journal of Science*, **282**, 1214–1231.

Berner, R.A., Sjöberg, E.L., Velbel, M.A., and Krom, M.D. (1980) Dissolution of pyroxenes and amphiboles during weathering. *Science*, **207**, 1205–1206.

Bowser, C.J. and Jones, B.F. (2002) Mineralogic controls on the composition of natural waters dominated by silicate hydrolysis. *American Journal of Science*, **302**, 582–662.

Brantley, S.L. (2005) Reaction kinetics of primary rock-forming minerals under ambient conditions. Pp. 73–117 in: *Surface and Ground Water, Weathering, and Soils* (J.I. Drever, editor). *Treatise on Geochemistry* vol. **5** (H.D. Holland and K.K. Turekian, editors). Elsevier-Pergamon, Oxford, UK.

Brantley, S.L. and Chen, Y. (1995) Chemical weathering rates of pyroxenes and amphiboles. Pp. 119–172 in: *Chemical Weathering Rates of Silicate Minerals* (A.F. White and S.L. Brantley, editors). Reviews in Mineralogy, vol. **31**, Mineralogical Society of America, Washington, D.C.

Bricker, O.P., Jones, B.F., and Bowser, C.J. (2005) Mass-balance approach to interpreting weathering reactions in watershed systems. Pp. 119–132 in: *Surface and Ground Water, Weathering, and Soils* (J.I. Drever, editor). *Treatise on Geochemistry* vol. **5** (H.D. Holland and K.K. Turekian, editors). Elsevier-Pergamon, Oxford, UK.

Casey, W.H., Banfield, J.F., Westrich, H.R., and McLaughlin, L. (1993) What do dissolution experiments tell us about natural weathering? *Chemical Geology*, **105**, 1–15.

Cole, W.F. and Lancucki, C.J. (1976) Montmorillonite pseudomorphs after amphibole from Melbourne, Australia. *Clays and Clay Minerals*, **24**, 79–83.

Colin, F., Nahon, D., Trescases, J.J., and Melfi, A.J. (1990) Lateritic weathering of pyroxenites at Niquelandia, Goias, Brazil: The supergene behavior of nickel. *Economic Geology*, **85**, 1010–1023.

Courchesne, F., Turmel, M.-C., and Beauchemin, P. (1996) Magnesium and potassium release by weathering in Spodosols: Grain surface coating effects. *Soil Science Society of America Journal*, **60**, 1188–1196.

Dahl, R. and Staehelin, A.A. (1989) High-pressure freezing for the preservation of biological structure: theory and practice. *Journal of Electron Microscopy Technique*, **13**, 165–174.

Delvigne, J. (1983) Micromorphology of the alteration and weathering of pyroxenes in the Koua Bocca ultramafic intrusion, Ivory Coast, West Africa. Pp. 57–68 in: *Pétrologie des Altérations et des Sols*, Volume II (D. Nahon and Y. Noack, editors). Sciences Géologiques, Mémoires (Strasbourg), vol. **72**.

Delvigne, J. (1990) Hypogene and supergene alterations of orthopyroxene in the Koua Bocca ultramafic intrusion, Ivory Coast. *Chemical Geology*, **84**, 49–53.

Delvigne, J. (1998) *Atlas of Micromorphology of Mineral Alteration and Weathering*. The Canadian Mineralogist, Special Publication **3**, 495 pp.

Eggleton, R.A. (1975) Nontronite topotaxial after hedenbergite. *American Mineralogist*, **60**, 1063–1068.

Eggleton, R.A. and Boland, J.N. (1982) Weathering of enstatite to talc through a sequence of transitional phases. *Clays and Clay Minerals*, **30**, 11–20.

Fisk, M.R., Popa, R., Mason, O.U., Storrie-Lombardi, M.C., and Vicenzi, E.P. (2006) Iron-magnesium silicate bio-weathering on Earth (and Mars?). *Astrobiology*, **6**, 48–68.

Hochella, M.F., Jr. and Banfield, J.F. (1995) Chemical weathering of silicates in nature: A microscopic perspective with theoretical considerations. Pp. 353–406 in: *Chemical Weathering Rates of Silicate Minerals* (A.F. White and S.L. Brantley, editors). Reviews in Mineralogy, vol. **31**, Mineralogical Society of America, Washington, D.C.

McKay, D.S., Gibson, E.K., Jr., Thomas-Keprta, K.L., Vali, H., Romanek, C.S., Clemett, S.J., Chillier, X.D.F., Maechling, C.R., and Zare, R.N. (1996) Search for past life on Mars: possible relic biogenic activity in Martian meteorite ALH84001. *Science,* **273**, 924–930.

Nahon, D.B. (1991) *Introduction to the Petrology of Soils and Chemical Weathering*. J. Wiley, New York.

Nahon, D.B. and Colin, F. (1982) Chemical weathering of orthopyroxenes under lateritic conditions. *American Journal of Science*, **282**, 1232–1243.

Nugent, M.A., Brantley, S.L., Pantano, C.G., and Maurice, P.A. (1998) The influence of natural mineral coatings on feldspar weathering. *Nature*, **395**, 588–591.

Pačes, T. (1983) Rate constants of dissolution derived from the measurements of mass balance in hydrological catchments. *Geochimica et Cosmochimica Acta*, **47**, 1855–1863.

Proust, D., Caillaud, J., and Fontaine, C. (2006) Clay minerals in early amphibole weathering: Tri- to dioctahedral sequence as a function of crystallization sites in the amphibole. *Clays and Clay Minerals*, **54**, 351–362.

Ransom, B. and Helgeson, H.C. (1994) Estimation of the standard molal heat capacities, entropies, and volumes of 2:1 clay minerals. *Geochimica et Cosmochimica Acta*, **58**, 4537–4547.

Schaetzl, R.J., Mikesell, L.R., and Velbel, M.A. (2006) Soil characteristics related to weathering and pedogenesis across a geomorphic surface of uniform age in Michigan. *Physical Geography*, **27**, 170–188.

Schott, J. and Berner, R.A. (1983) X-ray photoelectron studies of the mechanism of iron silicate dissolution during weathering. *Geochimica et Cosmochimica Acta*, **47**, 2233–2240.

Schott, J., Berner, R.A., and Sjoberg, E.L. (1981) Mechanism of pyroxene and amphibole weathering – I. Experimental studies of iron-free minerals. *Geochimica et Cosmochimica Acta*, **45**, 2123–2135.

Smyth, J.R. and Bish, D.L. (1988) *Crystal Structures and Cation Sites of the Rock-Forming Minerals*. Allen & Unwin, Boston, USA.

Velbel, M.A. (1985) Geochemical mass balances and weathering rates in forested watersheds of the southern Blue Ridge. *American Journal of Science*, **285**, 904–930.

Velbel, M.A. (1986) Influence of surface area, surface characteristics, and solution composition on feldspar weathering rates. Pp. 615–634 in: *Geochemical Processes at Mineral Surfaces* (J.A. Davis and K.F. Hayes, editors). ACS Symposium Series, No. **323**, American Chemical Society.

Velbel, M.A. (1989a) Weathering of hornblende to ferruginous products by a dissolution-reprecipitation mechanism: petrography and stoichiometry. *Clays and Clay Minerals*, **37**, 515–524.

Velbel, M.A. (1989b) Effect of chemical affinity on feldspar hydrolysis rates in two natural weathering systems. *Chemical Geology*, **78**, 245–253.

Velbel, M.A. (1990) Influence of temperature and mineral surface characteristics on feldspar weathering rates in natural and artificial systems: A first approximation. *Water Resources Research*, **26**, 3049–3053.

Velbel, M.A. (1993a) Formation of protective surface layers

during silicate-mineral weathering under well-leached, oxidizing conditions. *American Mineralogist*, **78**, 408–417.

Velbel, M.A. (1993b) Constancy of silicate-mineral weathering-rate ratios between natural and experimental weathering: Implications for hydrologic control of differences in absolute rates. *Chemical Geology*, **105**, 89–99.

Velbel, M.A. (2004) Laboratory and homework exercises in the geochemical kinetics of mineral-water reaction: rate law, Arrhenius activation energy, and the rate-determining step in the dissolution of halite. *Journal of Geoscience Education*, **52**, 52–59.

Velbel, M.A. (2007) Surface textures and dissolution processes of heavy minerals in the sedimentary cycle: examples from pyroxenes and amphiboles. Pp. 113–150 in: *Heavy Minerals in Use* (M. Mange and D. Wright, editors). Developments in Sedimentology, **58**, Elsevier, Amsterdam.

Wentworth, S.J., Gibson, E.K., Velbel, M.A., and McKay, D.S. (2005) Antarctic dry valleys and indigenous weathering in Mars meteorites: implications for water and life on Mars. *Icarus*, **174**, 382–395.

White, A.F. and Brantley, S.L. (2003) The effect of time on the weathering of silicate minerals: why do weathering rates differ in the laboratory and field? *Chemical Geology*, **202**, 479–506.

Wilson, M.J. (1986) Mineral weathering processes in podzolic soils on granitic materials and their implications for surface water acidification. *Journal of the Geological Society, London*, **143**, 691–697.

Wilson, M.J. (2004) Weathering of the primary rock-forming minerals; processes, products and rates. *Clay Minerals*, **39**, 233–266.

(*Received 4 August 2006; revised 10 October 2007; Ms. 1203*)